

Results from pp at 62.4 and 200 GeV with the BRAHMS experiment

F.Videbæk¹ for the BRAHMS experiment

¹ Brookhaven National Laboratory, NY 11973 Upton, New York, US

Abstract. Measurements of elementary pp collisions are essential for understanding heavy ion collisions. Results for pp collisions at 200 and 62.4 GeV are presented. At both energies NLO pQCD describes pion production well. The measured pion transverse single spin asymmetries are very large at 62.4 GeV and are reasonably well described by models relying on pQCD at transverse momenta larger than 1 GeV/c.

Keywords: pp spectra, RHIC, single spin asymmetry

PACS: 13.85.Ni,13.85.Hd,13.88+e,12.38Qk,25.75.-q

1. Introduction

One of the goals of the relativistic heavy ion program is to study the properties of matter at high temperature and high density. The explorations at the Relativistic Heavy Ion Collider (RHIC) indicate that at c.m. energies of 200 GeV per nucleon pair indeed such system is formed with novel properties as characterized through the particle production [1, 2, 3, 4]. Part of these conclusions rely on comparison to elementary pp collisions, where such nuclear effects should not be present. The RHIC experiments have also explored Au+Au and Cu+Cu collisions at 62.4 GeV, an intermediate energy between that at the SPS (18 GeV) and that where the bulk of the RHIC heavy ion program is performed at 200 GeV. The 62.4 GeV was chosen to match the highest energy where data were obtained in the ISR experiments. Thus, to minimize the systematic uncertainty for the comparisons to the heavy ion data a brief run with (polarized) pp at 62.4 GeV was carried out to collect pp reference data by the BRAHMS, PHENIX and STAR experiments. Thus, at this point in time an extensive set of pp reference data have been collected at these two energies.

In addition to the pp comparison data there is an extensive spin program at RHIC. It has long been envisioned that BRAHMS could contribute to these studies using the transversely polarized proton beams by measuring pions at large momenta

at forward angles. Part of run-5 and run-6 was dedicated to such measurements. There is current interest in understanding the large transverse single spin asymmetries (SSA) observed at moderate to large values of x_F in the energy range from 20 to 200 GeV in the framework of different approaches to pQCD. The main theoretical efforts to account for the observed SSA have focused on the role of transverse momentum dependent (TMD) partonic effects in the structure of the initial transversely polarized nucleon [5] and the fragmentation process of a polarized quark into hadrons [6]. Higher twist effects ("twist-3") arising from quark-gluon correlation effects have also been considered as a possible origin of SSA [7, 8]. To validate such an approach that is based on pQCD it is key to see how well pQCD describes inclusive data at high rapidities.

This contribution presents results of inclusive pp reactions at 200 and 62.4 GeV, and comparisons to pQCD at both energies. Transverse spin results from 62.4 and 200 GeV are also described and compared to model calculations.

2. Inclusive pp measurements

The data used for this analysis were collected with the BRAHMS detector system. The BRAHMS detector consists of two movable magnetic spectrometers, the Forward Spectrometer (FS) that can be rotated from 2.3° to 15° , and the Mid-Rapidity Spectrometer (MRS) that can be rotated from 34° to 90° degrees relative to the beam line, and several global detectors for measuring multiplicities and luminosity, and determining the interaction vertex, and providing a start time (T0) for time-of-flight measurement.

The MRS is a single-dipole-magnet spectrometer with a solid angle of $\approx 5msr$ and a magnetic bending power up to 1.2 Tm. Most of the data presented here were recorded at magnetic field settings of 0.4 and 0.6 Tm. The MRS contains two time projection chambers, TPM1 and TPM2 sitting in field free regions in front of and behind the dipole (D5). This assembly is followed by two highly segmented scintillator time-of-flight walls, one (TOFW) at 4.51 m and a second (TFW2) at either 5.58 m (90° setting) or 6.13 m (other angle settings).

The FS consists of 4 dipole magnets D1, D2, D3 and D4 with a bending power of up to 9.2 Tm. The spectrometer has 5 tracking stations T1 through T5, and particle identifying detectors: H2, a segmented time-of-flight wall, and a Ring Imaging Cherenkov Detector (RICH) [9]. Additional details on the BRAHMS experimental setup can be found in ref. [10].

The minimum bias trigger used to normalize these measurements is defined with a set of Cherenkov radiators (CC) placed symmetrically with respect to the nominal interaction point and covering pseudo-rapidities that range in absolute value from 3.26 to 5.25. This trigger required that at least one hit is detected in both sides of the array.

The present analysis was done with charged particles that originated from collisions of polarized protons with interaction vertices in the range of ± 40 cm. For

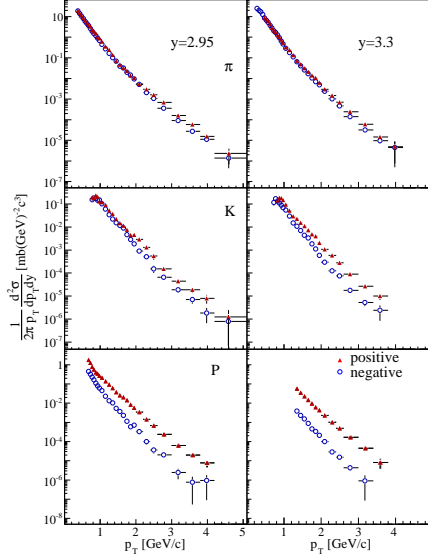


Fig. 1. Invariant cross section distributions for pion, kaons protons and anti-protons produced in p+p collisions at $\sqrt{s} = 200$ GeV at rapidities $y = 2.95$ (left panels) and $y = 3.3$ (right panels). In all panels, positive charged particles are shown with filled triangles and negative ones with open circles. The errors displayed in these plots are statistical.

the 200 GeV data invariant cross sections were extracted in narrow ($\Delta y = 0.1$) rapidity bins centered at $y = 2.95$ and $y = 3.3$, respectively. Narrow rapidity bins are required to reduce the effects of rapidly changing cross sections in particular at higher p_T . Each distribution is obtained from the merging of up to five magnetic field settings. The data are corrected for the spectrometer geometrical acceptance, multiple scattering, weak decays and absorption in the material along the path of the detected particles. Tracking and matching efficiencies for each of the 5 tracking stations in the spectrometer were calculated by constructing full tracks with only 4 stations and evaluating the efficiency in the 5th station. The overall efficiency is about 80-90% and is included in the extraction of the cross sections. Particles are identified by the RICH. The low momentum part of the proton spectra is measured using the RICH in veto mode.

Data for $y = 2.95$ and $y = 3.3$ are presented for pions, kaons and protons in Fig.1. The pions exhibit a power law behavior, and at high p_T the ratio π^-/π^+ is less than one indicating the increasing importance of the valence quarks. The \bar{p}/p ratio is much smaller than 1 p_T indicating that in the case of fragmentation the gluons cannot dominate the particle production.

The measured differential cross-sections are compared with NLO pQCD calculations [11] evaluated at equal factorization and renormalization scales, $\mu \equiv \mu_F =$

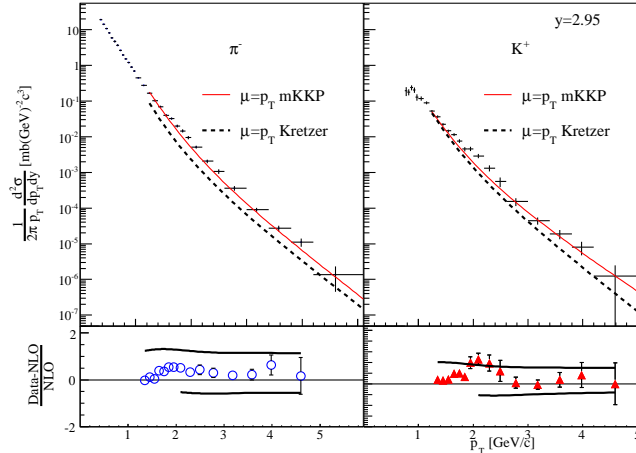


Fig. 2. Comparison of π^- and K^+ invariant spectra at rapidity 2.95 to NLO pQCD calculations at 200 GeV.

$\mu_R = p_T$. These calculations use the CTEQ6 parton distribution functions [12] and a modified version of the “Kniehl-Kramer-Potter” (KKP) set of fragmentation functions (FFs) [13] referred to here as mKKP, as well as the “Kretzer” (K) set [14]. The KKP set includes functions that fragment into the sums $\pi^+ + \pi^-$ and $K^+ + K^-$. Modifications were necessary to obtain functions producing the separate charges for both π and K . These modifications involve the following operations: to obtain the FFs producing π^+ , the functions that describe the fragmentation of favored light quarks u, \bar{d} into π^0 were multiplied by $(1+z)$ (e.g. $D_u^{\pi^0} = (1+z)D_u^{\pi^0}$ with $D_u^{\pi^0} = \frac{1}{2}D_u^{\pi^+ + \pi^-}$) where z is the fraction of the parton momentum carried by the hadron, and $D_u^{\pi^+}$ the function fragmenting u quarks into positive pions. The functions fragmenting unfavored quarks \bar{u}, d into π^0 are multiplied by $1-z$. The same operation is done for π^- , but this time the favored quarks are \bar{u} and d . The FFs of strange quarks and gluons are left unmodified. Similar modifications were applied to obtain FFs into K^+ and K^- , but this time, the starting functions were the ones fragmenting u, \bar{u}, s, \bar{s} into the sum $K^+ + K^-$. Figure 2 shows that the agreement between the NLO calculations that include the mKKP FFs and the measured pion cross section is remarkable (within 20% above 1.5 GeV/c). Similar good agreement was obtained for neutral pions at $y = 0$ [15] and at $y = 3.8$ [16] at RHIC. The agreement between the calculated and the measured kaon cross-sections is equally good. The difference between the mKKP and Kretzer parametrizations is driven by higher contributions from gluons fragmenting into pions. This difference has been identified as an indication that the gg and gq processes dominate the interactions at mid-rapidity [15]. The present results indicate that such continues to be the case at high rapidity. The calculation that uses the Kretzer set underestimates the pion yields by a factor of ~ 2 at all values of p_T while for positive kaons the agreement

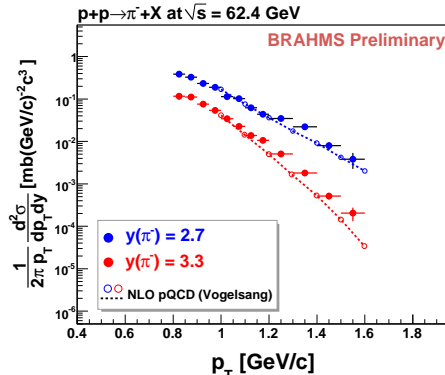


Fig. 3. Invariant cross section for π^- at rapidity 2.7 and 3.3 at 62.4 GeV. The curves are NLO pQCD calculations as described in the text.

is good at low momentum but deteriorates at higher momenta. Additional details as well as comparisons to p and \bar{p} spectra can be found in Ref.[17].

At 62.4 GeV, where the beam rapidity is 4.2, the spectrometer at forward angle samples produced particles that carries a significant fraction of the available momenta (31.2 GeV/c). Thus particle production is influenced by the kinematic limit. Data for identified charged hadrons were collected at $2.3^\circ, 3^\circ, 4^\circ$, and 6° . Figure 3 shows differential cross sections for π^- for rapidities 2.7 and 3.3. The cross sections changes rapidly with rapidity at high p_T where x_F values up to 0.5 are probed. The data are compared to NLO pQCD in the same figure. The calculation are done in the same manner as for the 200 GeV using the KPP fragmentation function evaluated at $\mu = p_T$ scale. The calculation describes the overall magnitude and shape quite well, though at the highest rapidity there is a tendency for the calculation to fall below the data at the highest p_T . This may be in agreement with the analysis[18] of 53 GeV π^0 data from the ISR at a fixed angle of 5° , comparable to the conditions for the present measurements (2.3° and 4°), but at larger x_F where NLO pQCD results falls considerably below the data and with increasing discrepancy with x_F . In contrast to the aforementioned paper we do, though, conclude that NLO pQCD gives a satisfactory description of the charged pion data at high rapidity.

3. Transverse Single Spin Asymmetries

The SSA is defined as a “left-right” asymmetry of produced particles from the hadronic scattering of transversely polarized protons off unpolarized protons. Experimentally the asymmetry can be obtained by flipping the spins of polarized protons, and is customarily defined as analyzing power A_N :

$$A_N = \frac{1}{\mathcal{P}} \frac{(N^+ - \mathcal{L}N^-)}{(N^+ + \mathcal{L}N^-)}, \quad (1)$$

where \mathcal{P} is the polarization of the beam, \mathcal{L} is the spin dependent relative luminosity ($\mathcal{L} = \mathcal{L}_+/\mathcal{L}_-$) and $N^{+(-)}$ is the number of detected particles with beam spin vector oriented up (down). The average polarization of the beam \mathcal{P} as determined from

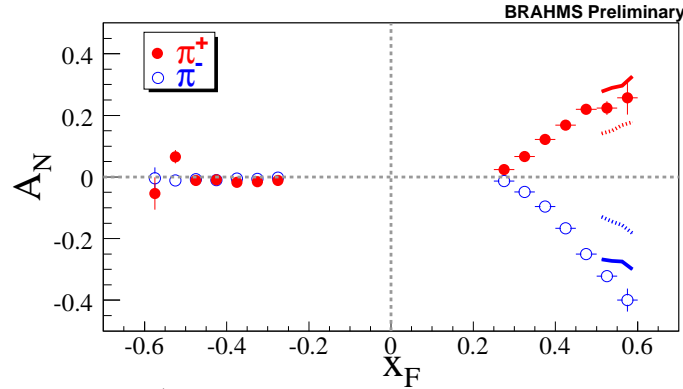


Fig. 4. A_N vs x_F for π^+ and π^- at 62.4 GeV for positive and negative x_F . Solid symbols are for π^+ and open for π^- . The curves are from the twist-3 calculations with (line) and without (broken) sea and anti-quark contribution. Predictions from the Siverson function calculation are shown as dotted lines.

the on-line CNI measurements is about 60% for run 6 (62.4 GeV) and about 45% for run 5 (200 GeV). The systematic error on the A_N measurements is estimated to be 20% including uncertainties from the beam polarization ($\sim 18\%$). The systematic error represents mainly scaling uncertainties on the values of A_N .

The production rate of pions in given p_T and x_F bins are determined in a similar way as that for inclusive spectra, except that acceptance and efficiency corrections are not performed since all of these will cancel out in the calculation of the quantities needed for determination of A_N .

The analyzing power A_N for charged pions, $A_N(\pi^+)$ and $A_N(\pi^-)$ at $\sqrt{s} = 62.4$ GeV as a function of x_F are shown in Fig. 4 using data taken at 2.3° and 3° . The p_T range covered is from about 0.6 GeV/c at the lowest x_F up to 1.5 GeV/c at the highest x_F . The measured A_N values show strong dependence with x_F reaching large asymmetries reaching up to $\sim 40\%$ at $x_F \sim 0.6$. The A_N values are positive for π^+ and negative for π^- and with approximately the same magnitude. The asymmetries and their x_F -dependence are qualitatively in agreement with the measurements from E704/FNAL.

The analyzing power A_N for charged pions, $A_N(\pi^+)$ and $A_N(\pi^-)$ at $\sqrt{s} = 200$ GeV as a function of x_F are shown in Fig. 5 using data taken at 2.3° and 4° . The kinematic range is quite different from the 62.4 GeV data. The x_F -range covered is from 0.15 to 0.35, while the p_T values covered by the measurements are much higher ranging from ~ 1 to 4 GeV/c. The left panel shows data from the 2.3° setting, while the right panel is for 4° . The latter for a given x_F represents a higher p_T value than for the 2.3° data. Overall the asymmetries are smaller for the higher p_T 's.

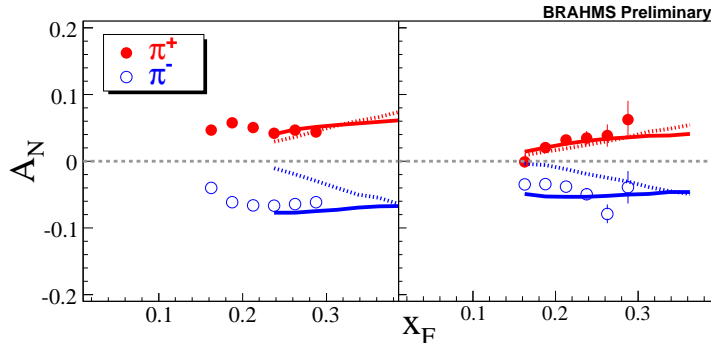


Fig. 5. A_N vs x_F for pions at 200 GeV. Solid symbols are for π^+ and open for π^- measured at 2.3° (left panel) and 4° (right panel). The curves are from the twist-3 calculations with (line) and without (broken) sea and anti-quark contributions. Predictions from the Siverson function calculation are shown as dotted lines.

Figure 4 compares $A_N(\pi)$ with a pQCD calculation in the range of $p_T > 1$ GeV/ c using “extended” twist-3 parton distributions [7] including the “non-derivative” contributions [19, 20]. In this framework, two calculations from the model are compared with the data: two valence densities (u_v, d_v) in the ansatz with and without sea- and anti-quark contribution in the model fit. The calculations describe the data within the uncertainties.

For the calculations shown in the figure, the dominant contributions to SSAs are from valence quarks, while sea- and anti-quark contributions on SSAs are sufficiently small that the current measurements are not able to quantitatively constrain these contributions. The data are also compared with calculations using the Siverson mechanism which successfully describe FNAL/E704 A_N data. The calculations compared with the data use valence-like Siverson functions [21, 22] for u and d quarks with opposite sign. The fragmentation functions used are from the KKP parameterization [13], but the Kretzer fragmentation function [14] gives similar results. The calculations shown with dotted lines in the figure underestimate A_N for both p_T ranges, which indicates that TMD parton distributions are not sufficient to describe the SSA data at 62.4 GeV. The same kind of calculations are compared to the 200 GeV data in Fig.5 yielding similar conclusions as for 62.4 GeV

4. Summary

In summary, unbiased invariant cross sections of identified charged particles as function of p_T were measured at high rapidity in p+p collisions at $\sqrt{s} = 200$ GeV and $\sqrt{s} = 62.4$ GeV. NLO pQCD calculations reproduce reasonably well the produced particle (pions and kaons) distributions. The SSA for inclusive pions were measured at forward rapidities at the same two energies. A twist-3 pQCD model of

A_N describes the x_F and energy dependence reasonable well. There are theoretical challenges in describing the data at both lower energy and lower p_T .

We thank Werner Vogelsang, Feng Yuan and Umberto D'Alesio for providing us with their calculations shown in this contribution and in forth coming publications. This work was supported by Brookhaven Science Associates,LLC under contract DE-AC02-98-CH10886 with the U.S. Department of Energy and by a sponsored grant from Renaissance Technologies Corporation.

References

1. I. Arsene *et al.*, BRAHMS Collaboration, *Nucl.Phys.* **A757** 1 (2005).
2. B. Back *et al.*, PHOBOS Collaboration, *Nucl.Phys.* **A757** 28 (2005).
3. J. Adams *et al.*, STAR Collaboration, *Nucl.Phys.* **A757** 102 (2005).
4. J. Acox *et al.*, PHENIX Collaboration, *Nucl.Phys.* **A757** 184 (2005).
5. D.Sivers, *Phys.Rev.* **D41** 83 (1990).
6. J.C.Collins, *Nucl.Phys.* **B396** 161 (1993).
7. J. Qiu and G. Sterman, *Phys. Rev.* **D59** 014004 (1999).
8. For a review, see J. Kodaira and K. Tanaka, *Prog. Theor. Phys.* **101** 191 (1999).
9. R. Debbé *et al.*, *Nucl. Instrum. Methods* **A570**, 216 (2007).
10. M. Adamczyk *et al.*, *Nucl. Instrum. Methods* **A499**, 437 (2003).
11. W. Vogelsang, private communication.
12. J. Pumplin *et al.*, *JHEP* 0207, 012 (2002); arXiv:hep-ph/0201195.
13. B.A. Kniehl *et al.*, *Nucl. Phys.* **B597** 337 (2001).
14. S. Kretzer *et al.*, *Eur. Phys. J.* **C22** 269 (2001).
15. S.S. Adler *et al.*, *Phys. Rev. Lett.* **91** 241803 (2003).
16. J. Adams *et al.*, *Phys. Rev. Lett.* **92** 171801 (2004).
Phys. Rev. **D67**, 054005 (2003).
17. I. Arsene *et al.*, BRAHMS Collaboration. accepted for publication in PRL, arXiv:hep-ex/0701041
18. C. Bourrely and J. Soffer, *Eur. Phys. J.* **C36** 371 (2004).
19. C. Kouvaris *et al.*, *Phys. Rev.* **D74** 1104013 (2006).
20. The calculations were provided by F. Yuan.
21. U. D'Alesio and F. Murgia, *Phys. Rev.* **D70** 074009 (2004), SPIN06 proceedings.
22. The calculations were provided by U. D'Alesio.